British Journal of Pharmacology

DOI:10.1111/j.1476-5381.2012.02125.x
www.brjpharmacol.org

RESEARCH PAPER

Functional and morphological properties of pericytes in suburothelial venules of the mouse bladder

Hikaru Hashitani[1], Retsu Mitsui[1], Yuki Shimizu[1], Ryuhei Higashi[2] and Keiichiro Nakamura[2]

[1]*Department of Cell Physiology, Nagoya City University Graduate School of Medical Sciences, Nagoya, Japan, and* [2]*Division of Microscopic and Developmental Anatomy, Kurume University School of Medicine, Kurume, Japan*

Correspondence
Hikaru Hashitani, Department of Cell Physiology, Nagoya City University Graduate School of Medical Sciences, Nagoya 467-8601, Japan. E-mail: hasitani@med.nagoya-cu.ac.jp

Keywords
pericyte; Ca^{2+} transient; microcirculation

Received
2 May 2012
Revised
19 June 2012
Accepted
26 July 2012

BACKGROUND AND PURPOSE

In suburothelial venules of rat bladder, pericytes (perivascular cells) develop spontaneous Ca^{2+} transients, which may drive the smooth muscle wall to generate spontaneous venular constrictions. We aimed to further explore the morphological and functional characteristics of pericytes in the mouse bladder.

EXPERIMENTAL APPROACH

The morphological features of pericytes were investigated by electron microscopy and fluorescence immunohistochemistry. Changes in diameters of suburothelial venules were measured using video microscopy, while intracellular Ca^{2+} dynamics were visualized using Fluo-4 fluorescence Ca^{2+} imaging.

KEY RESULTS

A network of α-smooth muscle actin immunoreactive pericytes surrounded venules in the mouse bladder suburothelium. Scanning electron microscopy revealed that this network of stellate-shaped pericytes covered the venules, while transmission electron microscopy demonstrated that the venular wall consisted of endothelium and adjacent pericytes, lacking an intermediate smooth muscle layer. Pericytes exhibited spontaneous Ca^{2+} transients, which were accompanied by phasic venular constrictions. Nicardipine (1 μM) disrupted the synchrony of spontaneous Ca^{2+} transients in pericytes and reduced their associated constrictions. Residual asynchronous Ca^{2+} transients were suppressed by cyclopiazonic acid (10 μM), 2-aminoethoxydiphenyl borate (10 μM), U-73122 (1 μM), oligomycin (1 μM) and SKF96365 (10 μM), but unaffected by ryanodine (100 μM) or YM-244769 (1 μM), suggesting that pericyte Ca^{2+} transients rely on Ca^{2+} release from the endoplasmic reticulum via the $InsP_3$ receptor and also require Ca^{2+} influx through store-operated Ca^{2+} channels.

CONCLUSIONS AND IMPLICATIONS

The pericytes in mouse bladder can generate spontaneous Ca^{2+} transients and contractions, and thus have a fundamental role in promoting spontaneous constrictions of suburothelial venules.

Abbreviations

2-APB, 2-aminoethoxydiphenyl borate; CPA, cyclopiazonic acid; CCCP, carbonyl cyanide 3-chlorophenylhydrazone; CRAC, Ca^{2+} release-activated Ca^{2+} channels; InsP3, inositol 1,4,5-trisphosphate; LNA, L-nitro-arginine; NCX, Na^{+}-Ca^{2+} exchanger; PDGFR, platelet-derived growth factor receptor; SERCA, sarco/endoplasmic reticulum Ca^{2+}-ATPase; α-SMA, α-smooth muscle actin; YM-244769, N-(3-aminobenzyl)-6-{4-[(3-fluorobenzyl)oxy] phenoxy}nicotinamide

Introduction

The urinary bladder is a unique organ that is capable of accommodating large volumes of urine with remarkably little rises in intravesical pressure. This functional feature largely relies on the high compliance properties of the detrusor smooth muscle cells that do not develop any substantial passive tension even when their lengths increase several-fold during bladder filling (Brading, 1987). Because intravesical pressure during bladder filling does not exceed capillary pressure, normal bladders maintain their circulation, so that the blood supply only transiently drops during voiding (Greenland and Brading, 1996). Several specializations of the vasculature appear to maintain blood flow in the bladder wall during distension. Blood vessels in the bladder wall are characterized by their winding arrangement, which prevents them from being stretched in their longitudinal direction during bladder filling (Sarma, 1981). Thus, they are capable of maintaining their diameter so that the resistance against blood flow is not increased. However, a prolonged reduction in the blood flow occurs in obstructed bladders during voiding, and significant reductions in the blood flow are detected in non-compliant bladders even during the filling phase (Greenland and Brading, 2001).

Overactive bladder is a highly prevalent disorder that increases with age, although its cause or aetiology is mostly unknown. Complex pathological changes in the signalling transmission from the urothelium to afferent nerves have been proposed to be a primary cause of overactive bladder, particularly with urgency during the storage phase (Yoshimura, 2007). It is also likely that overactive bladder could be caused by ischaemic and reperfusion damage to the cells in the bladder wall as a consequence of bladder outlet obstruction (Gosling *et al.*, 2000) or circulation dysfunction that is accompanied by aging and atherosclerosis (Azadzoi *et al.*, 1999; Yoshida *et al.*, 2010). Therefore, we propose that the suburothelial microvasculature may play a critical role in maintaining normal bladder function. The beneficial effects of α-adrenoceptor antagonists on bladder storage symptoms suggest extraprostatic targets of α-adrenoceptor antagonists, including the urothelium and afferent nerves (Sun *et al.*, 2002; Yokoyama *et al.*, 2006). In addition, α-adrenoceptor antagonists may also improve bladder circulation to preserve cell functions. Similarly, mirabegron (YM178), a β_3-adrenoceptor agonist, which has recently been approved for clinical use as a novel medicine for overactive bladder, may also exert its action by improving microcirculation within the bladder wall (Takasu *et al.*, 2007).

We have recently reported that sunburothelial venules of the rat bladder exhibit spontaneous phasic constrictions that may be beneficial for maintaining venular drainage (Hashitani *et al.*, 2011). Suburothelial venules, but not arterioles, developed spontaneous phasic constrictions at a frequency of 3–5 min^{-1}. The mechanisms underlying these spontaneous constrictions appear to involve the firing of spontaneous transient depolarizations resulting from the opening of Ca^{2+}-activated Cl^- channels that activate L-type voltage-gated Ca^{2+} channels to trigger action potential discharge. Ca^{2+} imaging *in situ* revealed that both spindle-shaped smooth muscle cells and stellate-shaped pericytes (perivascular cells) exhibited spontaneous Ca^{2+} transients resulting from Ca^{2+} release via inositol 1,4,5-trisphosphate ($InsP_3$) receptor Ca^{2+} channels. However, unlike the rabbit urethra or mouse renal pelvis where smooth muscle Ca^{2+} transients were readily abolished by blockers for L-type Ca^{2+} channels (Hashitani and Suzuki, 2007; Lang *et al.*, 2007), both cell types were capable of generating Ca^{2+} transients in the presence of nicardipine. Thus, we were not able to determine which cell population may play a fundamental role in driving this system.

In the present study, we aimed to identify the morphological and functional characteristics of pericytes in the mouse bladder, focusing on their role in generating spontaneous venular constrictions. Immunohistochemical study and electron microscopy were carried out to identify the cells displaying the spontaneous Ca^{2+} transients. The properties of the spontaneous phasic constrictions of suburothelial venules were investigated by monitoring changes in their diameter, while intracellular Ca^{2+} dynamics of cells within the venular wall were visualized using Fluo-4 Ca^{2+} imaging.

Methods

Tissue preparation

Male BALB/c mice, aged 8–12 weeks, were anaesthetized by being exposed to vapours of sevoflurane, and exsanguinated by decapitation according to procedures approved by The Experimental Animal Committee of the Nagoya City University Graduate School of Medical Sciences (the total number of mice used was 120). The bladder was removed and pinned out in a dissecting dish with the urothelial side uppermost. The mucosal layer was dissected away from the detrusor smooth muscle layer, and then the urothelial layer was carefully removed using ophthalmology scissors leaving the suburothelial layer containing the microvaculature (lamina propria). The small intestine was used for positive controls of Kit, Ano-1 and PEGFRα immnohistochemistry.

Freshly isolated interstitial cells taken from longitudinal smooth muscle preparations of the rabbit urethra (see details in Hashitani *et al.*, 2010) were used for positive control of YM244769, a blocker for the type 3 isoform of the Na^+-Ca^{2+} exchanger (NCX3).

All studies involving animals are reported in accordance with the ARRIVE guidelines (Kilkenny *et al.*, 2010; McGrath *et al.*, 2010).

Immunohistochemistry

The mouse bladder was immersed in PBS at 4°C. Tissue was cut, opened and the muscle layer removed with sharp tweezers under a dissection microscope. The remained mucosa was pinned flat. For α-smooth muscle actin (α-SMA) or NG2 chondroitin sulphate proteoglycan immunostaining, tissues were immersed in fixative containing 2% formaldehyde and 15% saturated picric acid in 0.1 M phosphate buffer (pH 7.4) for 10 min. The pins were removed and the tissue was then immersed in the same fixative overnight at 4°C. The fixed tissues were washed in DMSO (10 min × 3) and then in PBS (10 min × 3). For immunostaining using other antibodies (see below), flattened mucosal tissues were fixed in acetone for 10 min and washed in PBS.

Mucosal whole mounts were incubated with 0.3% Triton X-100 in PBS for 10 min, incubated with Block Ace (Dainippon Seiyaku, Osaka, Japan) for 20 min and incubated with primary antibodies for 4 days at 4°C. Tissues were then incubated with biotinylated anti-rabbit antibody for 30 min at room temperature only when rabbit primary antibody was used. Whole mounts were incubated with secondary antibodies or Alexa488- or Cy3-conjugated streptavidin for 2 h at room temperature. Preparations were coverslipped with Vectashield (Vector Laboratories, Burlingame, CA, USA) and examined using a confocal laser scanning microscope (LSM 5 PASCAL, Zeiss, Hertfordshire, UK).

Antibodies used in the present study were as follows: mouse monoclonal antibody for α-SMA (1:1000, clone 1A4, Sigma, St Louis, MO, USA), rabbit anti-von Willebrand factor antibody (vWF; 1:400, Abcam, Cambridge, UK), rabbit anti-NG2 chondroitin sulphate proteoglycan antibody (1:500, Millipore, Billerica, MA, USA), rat monoclonal antibody for PDGF receptor β (1:500 or 1:100, clone APB5, eBioscience, San Diego, CA, USA), rat monoclonal antibody for PDGF receptor α (1:500, clone APA5, BioLegend, San Diego, CA, USA), rabbit anti-Anoctamin-1 (ANO1) antibody (1:100, Abcam), rat monoclonal antibody for c-Kit (1:1000, clone ACK2, eBioscience), Cy-3-conjugated goat anti-mouse IgG antibody (2.5 μg·mL^{-1}, Jackson ImmunoResearch, West Grove, PA, USA), biotinylated swine anti-rabbit IgG antibody (1:300, Dako, Carpinteria, CA, USA), Alexa488-conjugated streptavidin (10 μg·mL^{-1}, Jackson ImmunoResearch), Cy3-conjugated streptavidin (4.5 μg·mL^{-1}, Jackson ImmunoResearch), FITC-conjugated anti-rat IgG antibody (1:100, Dako). Primary antibodies were diluted in PBS containing 2% BSA and 0.3% triton X-100, and secondary antibodies were diluted in PBS containing 2% BSA.

Transmission electron microscopy

An anaesthetized mouse was perfused through the left ventricle of the heart with PBS (4°C) and then with a fixative (phosphate buffer containing 4% paraformaldehyde and 3% glutaraldehyde, pH 7.4, 4°C). The small pieces of bladder tissue were immersed in the same fixative for 2 h at 4°C and rinsed in phosphate buffer. Tissue was immersed in 1% osmium tetroxide for 2 h at 4°C, rinsed in distilled water and incubated with uranyl acetate overnight. Tissue was dehydrated in a graded series of ethanol and embedded in Epon epoxy resin. Ultrathin sections were cut with an ultramicrotome (Reichert, Saarland, Germany) and immersed in uranyl acetate and then in lead citrate. Specimens were observed with a transmission electron microscope (JEM-1011J, JEOL, Peabody, MA, USA).

Scanning electron microscopy

For the complete removal of connective tissue matrices including collagen and elastic fibres, dissected specimens were treated according to the KOH digestion method as follows: after being rinsed in 0.1 M phosphate buffer (pH 7.4), tissues were placed in 5N KOH for 15 min at 60°C, and rinsed several times in buffer (pH 7.4). Specimens were then immersed in 1% osmium tetroxide solution for 1 h, dehydrated through a graded series of acetone and freeze-dried in t-butylalcohol. They were then sputter coated with gold, and examined in a Hitachi S-800 scanning electron microscope (Tokyo, Japan) operated at an accelerating voltage of 20 kV.

Video imaging with Diamtrak

Suburothelial preparations were pinned out on a Sylgard plate at the bottom of recording chamber (volume, approximately 1 mL), which was mounted on the stage of an inverted microscope attached with a video camera. Preparations were superfused with oxygenated warmed (35°C) PSS at a constant flow rate (about 2 mL·min^{-1}) during all functional experiments. Changes in the diameter of suburothelial venules were monitored with a video camera, and analysed in real-time using Diamtrak Edge-tracking software (Neild, 1989).

Intracellular calcium imaging

Suburothelial preparations were incubated in low Ca^{2+} PSS ($[Ca^{2+}]_o$ = 0.1 mM) containing 1 μM fluo-4 AM (special packaging, Dojindo, Kumamoto, Japan) and cremphor EL (0.01%, Sigma) for 10–20 min at 35°C. Following incubation, the recording chamber was mounted on the stage of an upright epifluorescence microscope (BX51WI, Olympus, Tokyo, Japan) equipped with a back-thinned electron multiplying CCD camera (C9100-13, Hamamatsu Photonics, Hamamatsu, Japan). Preparations were superfused with dye-free PSS, viewed with a water immersion objective (UMPlanFL ×20 or LUMPlanFL ×60, Olympus) and illuminated at 495 nm. Fluorescence emissions were captured through a barrier filter above 515 nm, and images were obtained every 47–200 ms (frame interval) with an exposure time of 30–70 ms using a micro-photoluminescence measurement system (AQUACOSMOS, Hamamatsu Photonics). Relative amplitudes of Ca^{2+} transients were expressed as $\Delta F_t/F_0 = (F_t - F_0)/F_0$, where F_t is the fluorescence generated by an event, and baseline F_0 is the basal fluorescence.

Solutions

The composition of PSS was (in mM): Na^+ 137.5, K^+ 4.7, Ca^{2+} 2.5, Mg^{2+} 1.2, HCO_3^- 15.5, $H_2PO_4^-$ 1.2, Cl^- 134 and glucose 15. The pH of PSS was 7.2 when bubbled with 95% O_2 and 5% CO_2, and the measured pH of the recording bath was approximately 7.4.

Drugs used were 2-aminoethoxydiphenyl borate (2-APB), atropine, carbonyl cyanide 3-chlorophenylhydrazone (CCCP), cyclopiazonic acid (CPA), guanethidine, nicardipine, L-nitro-arginine (LNA), oligomycin, phentolamine, ryanodine, SKF96365, tetrodotoxin, U-73122, U-73433 and wortmannin (from Sigma). YM-244769 was synthesized by Professor T. Iwamoto (Fukuoka University, Japan). Atropine, guanethidine, LNA, phentolamine and tetrodotoxin were dissolved in distilled water, and 2-APB, CPA, nicardipine, ryanodine, SKF96365, U-73122, U-73433 and YM-244769 were dissolved in DMSO. The final concentration of the solvents above in the PSS did not exceed 1:1000.

Calculations and statistics

The following parameters of spontaneous events were measured: peak amplitude, measured as the value from the resting level to the peak of events; half-duration, measured as the time between 50% peak amplitude on the rising and falling

phases; frequency (min^{-1}) which was calculated as an average over 3–5 min of recording.

Measured values were expressed as mean ± SD. Statistical significance was tested using paired *t*-test, and considered significant if $P < 0.05$.

All drug/molecular target nomenclature conforms to BJP's *Guide to receptors and channels* (GRAC), 5th edition (Alexander *et al.*, 2011).

Results

Scanning electron microscopy of suburothelial venules

Close examination of the cytoarchitecture of suburothelial venules using scanning electron microscopy demonstrated that the mural surface of venules of <100 µm diameter consisted of pericytes (Figure 1A,B). As venules increased in diameter to >100 µm, flat ribbon-like smooth muscle cells that circumferentially orientated around the vessel wall were also apparent (Figure 1C).

Transmission electron microscopic feature of suburothelial venules

Transmission electron microscopy of cross-sections of the suburothelial microvasculature revealed that arterioles consist of an inner endothelial cell layer and outer smooth muscle cell layer (Figure 2A). Arteriolar smooth muscle cells were surrounded by nerve bundles and long, thin processes of fibroblast that were characterized by the lack of a basal membrane.

In contrast, the venular wall consists of an inner layer of endothelium and adjacent pericytes (Figure 2B). Pericytes and endothelial cells were frequently in close proximity, although no specialized gap junctions or other junctional structures were evident. However, fusion or close apposition of pericyte plasma and endothelium membranes was abundant especially in their processes. Pericytes are characterized by numerous caveolae, distinct basal lamina and heterogeneous fibres in the cytoplasm (Figure 2C).

Immunohistochemical properties of pericytes

Venular pericytes extended several processes to form a cellular network were immunoreactive for α-SMA (Figure 3A). Microvasculatures could be detected by immunohistocemistry for von Willebrand factor, an endothelial cell marker (Figure 3B), but such images of endothelium were distinct from the α-SMA-positive network of pericytes. NG2 chondroitin sulphate proteoglycan, a marker for vascular mesenchymal cells including pericytes, was detected in the arterial smooth muscles as well as capillary pericytes but not in venular pericytes (Figure 3C,D).

Venular pericytes were not immunoreactive for the markers of interstitial cells of *Cajal* (ICC) (c-Kit and Ano-1) or 'fibroblast-like cells' (PDGFRα) in the gut (data not shown). Specific binding of antibodies for c-Kit and Ano-1 or PDGFRα for interstitial cells of *Cajal* or 'fibroblast-like cells', respectively, was confirmed in the mouse small intestine.

Distinct immunoreactivity for PDGFRβ, which are expressed in capillary pericytes, was not detected in the pericytes of venule (data not shown).

Spontaneous constrictions of the suburothelial venules

Suburothelial venules (diameter ranging from 40 to 110 µm with a mean of 60.1 ± 20.2 µm, $n = 33$) generated spontaneous phasic constrictions (Figure 4A) that were not affected by atropine (1 µM, $n = 3$), phentolamine (1 µM, $n = 3$), guanethidine (10 µM, $n = 3$) or tetrodotoxin (1 µM, $n = 3$). Spontaneous venular constrictions occurred at a frequency ranging from 2.5 to 9.3 min^{-1}, with a mean value of 5.3 ± 1.6 min^{-1}, $n = 33$). These contractions resulted in a mean reduction in venular diameter of 23.9 ± 5.8% (ranging from 14.3 to 34.8%), with a mean half-amplitude duration of 4.2 ± 1.1 s ($n = 33$).

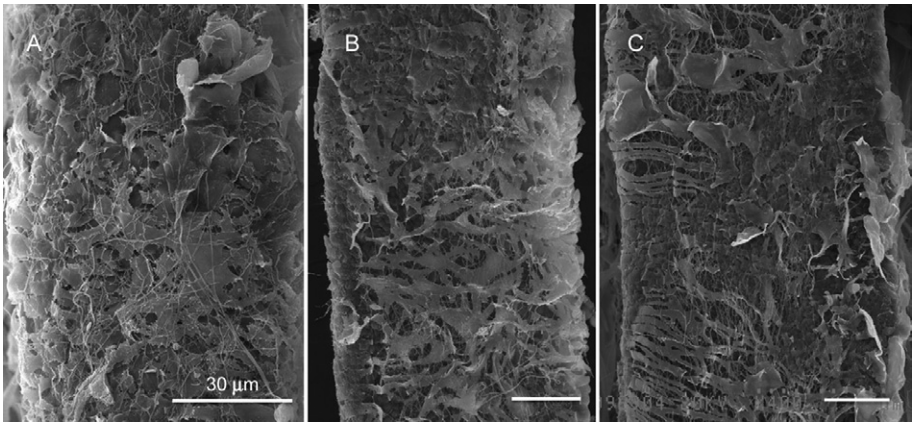

Figure 1

Scanning electron microscopy of suburothelial venules. Adventitial aspects of suburothelial venules of different diameter. A portion of venule, 60 µm in diameter, was surrounded by stellate-shaped pericytes (A). Stellate-shaped pericytes formed a network covering the outer surface of the vessel in another portion of venule, 100 µm in diameter (B). Smooth muscle cells in the most proximal portion of the venule 150 µm in diameter appeared like a piece of flat tape and were arranged in a circular direction (C).

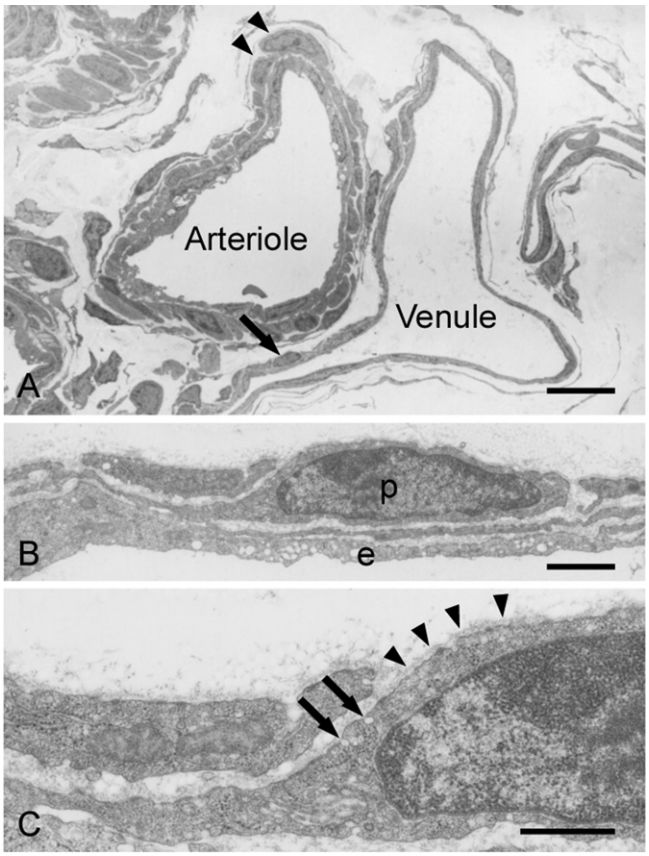

Figure 2

Electron microscopic characteristics of pericytes. Transmission electron microscopy showing a cross-section of a venule and arteriole (A). Note that the arteriole consists of inner endothelial layer and adjacent outer smooth muscle layer (arrowheads), while the venule lacks a smooth muscle layer. A pericyte in the venular wall is indicated by an arrow. The enlarged image of this pericyte is presented in (B). Venular wall consists of an inner layer of endothelium (e) and pericytes (p) that are characterized by their long processes. At a higher magnification, pericytes are characterized by numerous caveolae (arrows) and distinct basal lamina (arrowheads) (C). Heterogeneous fibres are abundant in the cytoplasm of pericytes, particularly in their processes. Scale bars: 10 μm (A), 1 μm (B) and 500 nm (C).

The effect of nicardipine, a dihydropyridine antagonist of L-type Ca^{2+} channels, was examined to test the role of voltage-dependent Ca^{2+} entry in spontaneous venular constrictions. Venular constrictions were progressively suppressed by nicardipine (1 μM) and this was associated with a sustained dilatation of the venules (n = 5, Figure 4B). In the presence of nicardipine (1 μM), small spontaneous constrictions occurred locally (Figure 4C,D). These non-propagating constrictions occurred with a mean frequency of 13.9 ± 2.4 min^{-1} and resulted in a mean reduction in venular diameter of 6.7 ± 1.6% (n = 5).

The role of the sarco-endoplasmic reticulum in generating spontaneous venular constrictions was examined using CPA, an inhibitor of sarco-endoplasmic reticulum Ca^{2+} ATPase (SERCA). CPA (10 μM) abolished spontaneous venular constrictions and caused a transient dilatation that was followed by a sustained constriction (n = 5, Figure 4E). After the withdrawal of CPA, the diameter of the venules gradually returned to its original level; spontaneous constrictions were slower to recover over a further 5–10 min. LNA (10 μM), an NOS inhibitor, increased the frequency of spontaneous constrictions (mean 5.3 ± 1.6 min^{-1} in control, 9.2 ± 1.8 min^{-1} in LNA, $P < 0.05$), associated with a reduction of venular diameter (n = 6). In preparations that had been treated with LNA for 20 min, CPA caused a sustained constriction and completely suppressed spontaneous constrictions (n = 4, Figure 4F).

Spontaneous Ca^{2+} transients of perivascular interstitial cells

Ca^{2+} imaging experiments revealed that the predominant cells exhibiting spontaneous Ca^{2+} transients were stellate-shaped pericytes, which formed an extensive network surrounding the venular lumen (Figure 5A,B). Synchronous Ca^{2+} transients within this pericyte network were associated with phasic constrictions (Supporting Information Video S1). As tight pinning did not prevent tissue distortion and loss of image focus, control parameters of spontaneous Ca^{2+} transients were recorded in preparations which had been pretreated with wortmannin (1 μM), an inhibitor of myosin light-chain kinase (Burke et al., 1996). Wortmannin greatly diminished these spontaneous constrictions, but did not affect either the frequency or synchrony of these Ca^{2+} transients, thus allowing the recording of Ca^{2+} signals from individual pericytes (Supporting Information Video S2). Spontaneous Ca^{2+} transients of pericytes (Figure 5C,D) occurred at a frequency of 4.4 ± 1.1 min^{-1} and had an amplitude and a half-duration of 1.4 ± 0.24$\Delta F_t/F_0$ and 4.8 ± 0.8 s, respectively (n = 16). Although we were not able to convincingly determine the effect of wortmannin on the amplitude of spontaneous Ca^{2+} transients, we tested if wortmannin suppressed the asynchronous Ca^{2+} transients in nicardipine-treated preparations (see below).

As previously reported in suburothelial venules of the rat bladder (Figure 5E; Hashitani *et al.*, 2011), nicardipine (1 μM) reduced the amplitude of pericyte Ca^{2+} transients in wortmannin-treated preparations to 21.3 ± 2.5% of control values (from 1.5 ± 0.38 to 0.32 ± 0.097$\Delta F_t/F_0$, n = 6). In the absence of wortmannin, pericytes developed asynchronous Ca^{2+} transients in 1 μM nicardipine that occurred at a frequency of 2.9 ± 0.83 min^{-1}, and had an amplitude of 0.96 ± 0.36$\Delta F_t/F_0$ and a half-duration of 2.7 ± 0.57 s (n = 21, Figure 6A,B). Asynchronous Ca^{2+} transients in pericytes were visualized in both their cell bodies and their processes (Supporting Information Video S3). On some occasions, Ca^{2+} transients spread through their processes to adjacent cells.

Consistent with the scanning electron microscopic observations, spindle-shaped smooth muscle cells exhibiting spontaneous Ca^{2+} transients were only observed in the most proximal portions of venules with diameters >100 μm where stellate-shaped pericytes were also distributed (Figure 6C,D). Smooth muscle Ca^{2+} transients occurred at a frequency of 3.3 ± 0.74 min^{-1}, had an amplitude of 0.83 ± 0.28$\Delta F_t/F_0$ and a half-duration of 2.9 ± 0.47 s (n = 7, Figure 6A, B). As the aim of this study was to explore the function of pericytes, the properties of smooth muscle cells in venules >100 μm were not examined further.

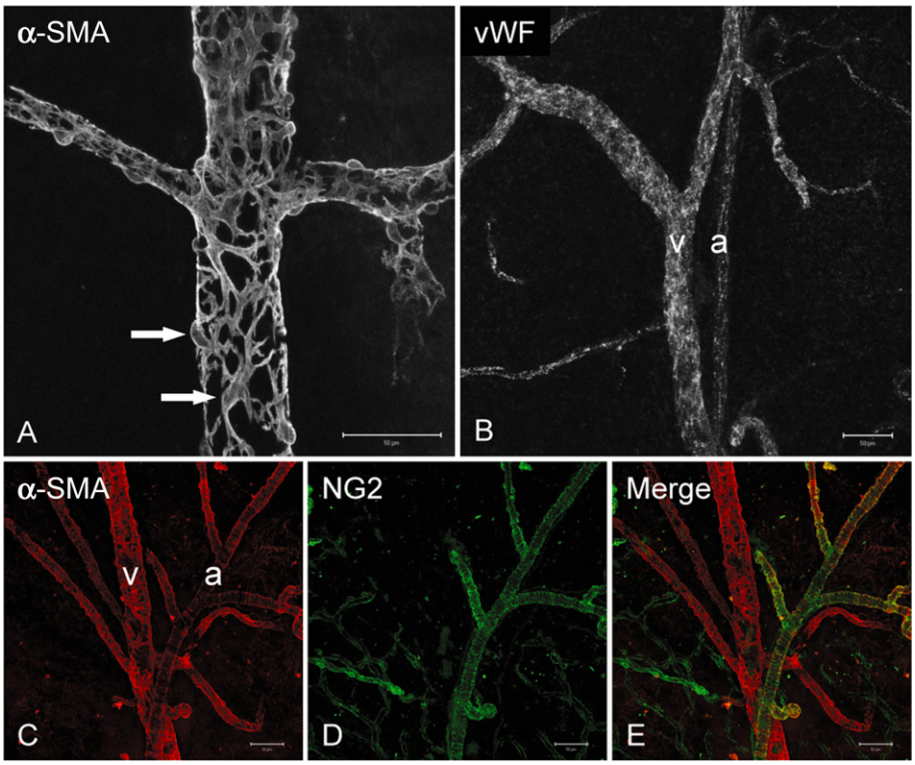

Figure 3

Immunohistochemical characteristics of pericytes. α -Smooth muscle actin (α-SMA) staining revealed a network of stellate-shaped pericytes that appear to be connected to each other via their processes (A). Note that pericytes have little cytoplasm around the nucleus (arrows) and a number of thin processes. Immunostaining for von Willebrand factor (vWF) revealed a distinct pattern of endothelial staining in both arteriole (a) and venule (v) (B). Both arteriole (a) and venule (v) in the mucosa were immunoreactive for α-SMA (C). NG2 chondroitin sulphate proteoglycan (NG2)-immunoreactivity was detected in the arteriole but not venule (D). The arteriole positive for both α-SMA and NG2 are shown in yellow in a merged image (E). Scale bars: 50 μm.

Role of SERCA in generating spontaneous Ca^{2+} transients of pericytes

As heterogeneous cell populations distributed in smooth muscle organs operate different Ca^{2+} mobilizing mechanisms to generate spontaneous activity, cellular mechanisms underlying the generation of nicardipine-resistant, asynchronous Ca^{2+} transients of pericytes were investigated using a standard pharmacological approach.

CPA (10 μM) increased basal Ca^{2+} levels ($0.39 \pm 0.097\Delta F_t/F_0$, $n = 6$) in pericytes in venules <100 μm and prevented the generation of spontaneous Ca^{2+} transients (Figure 7A), indicating the fundamental role of SERCA activity in sustaining the spontaneous Ca^{2+} transients of pericytes.

CCCP (1 μM), which disrupts electrical gradient across mitochondrial inner membrane, abolished spontaneous Ca^{2+} transients associated with a small rise in the Ca^{2+} basal level ($n = 4$, Figure 7B). Oligomycin (1 μM), an inhibitor of mitochondrial ATP synthesis, also effectively prevented spontaneous Ca^{2+} transients with a marginal rise in the Ca^{2+} basal level ($n = 7$, Figure 7C), suggesting that mitochondrial ATP production may be a major energetic source for SERCA operation in venular pericytes.

Role of intracellular Ca^{2+} release in generating spontaneous Ca^{2+} transients of pericytes

Open state block of ryanodine receptor Ca^{2+} release channels with ryanodine (100 μM for 30 min) did not affect either the frequency (2.9 ± 0.72 min^{-1} in control, 3.0 ± 0.37 min^{-1} in ryanodine, $P > 0.05$, $n = 5$) or amplitude ($0.94 \pm 0.18\Delta F_t/F_0$ in control, $1.0 \pm 0.25\Delta F_t/F_0$ in ryanodine, $P > 0.05$) of spontaneous Ca^{2+} transients in nicardipine (1 μM, Figure 8A,B). 2-APB (10 μM), a non-selective blocker of $InsP_3$ receptor Ca^{2+} release channels, progressively suppressed spontaneous Ca^{2+} transients until their generation ceased (Figure 8C), irrespective of the presence ($n = 3$) or absence ($n = 5$) of pretreatment with ryanodine (100 μM for 30 min).

U-73343 (1 μM), an inactive structural analogue of U-73122 that has little or no effect on phospholipase C, did not change either the frequency (4.7 ± 0.91 min^{-1} in control, 4.8 ± 0.99 min^{-1} in U-73343, $P > 0.05$, $n = 5$) or amplitude ($0.83 \pm 0.2\Delta F_t/F_0$ in control, $0.79 \pm 0.16\Delta F_t/F_0$ in U-73343, $P > 0.05$) of the spontaneous Ca^{2+} transients (Figure 8D). In contrast, inhibition of phospholipase C with U-73122 (1 μM) reduced the amplitude and frequency of spontaneous Ca^{2+} transients and prevented their generations (Figure 8E),

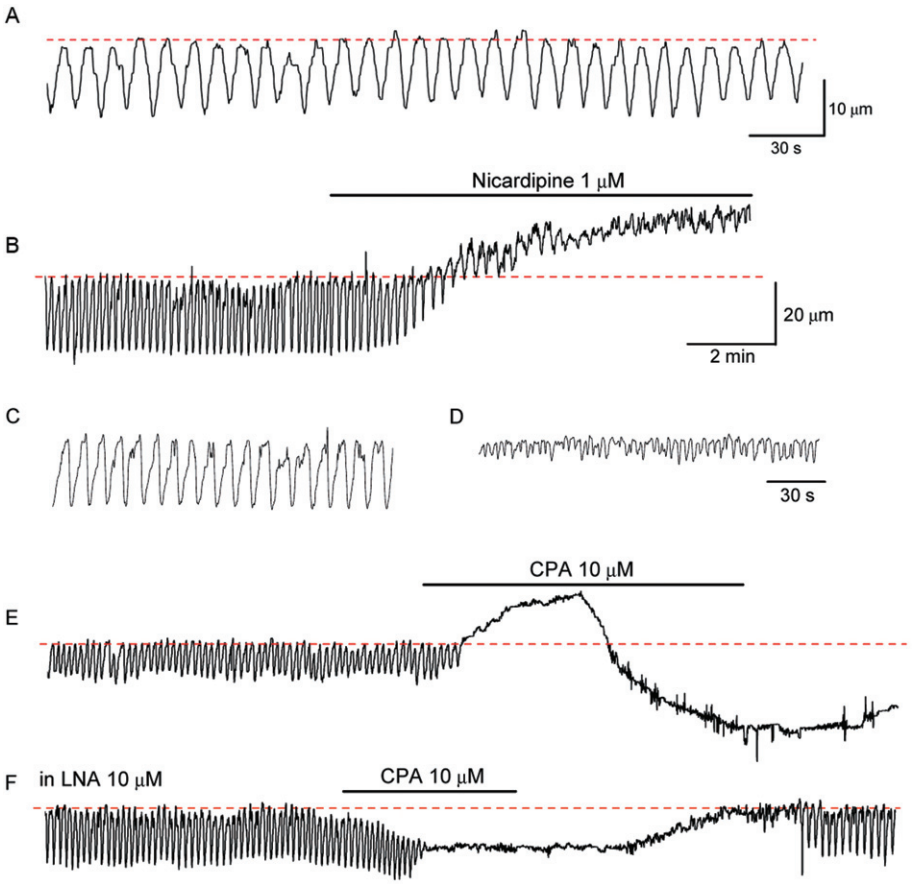

Figure 4

Spontaneous constrictions in the suburothelial venules. Suburothelial venules of the mouse bladder generate spontaneous constrictions as indicated by transient reductions in the venular diameter (A). Nicardipine largely suppressed these spontaneous constrictions with a dilatation of the venule (B). In the presence of nicardipine, smaller, localized constrictions were generated (C, control; D, in nicardipine). CPA (10 μM) abolished all spontaneous constrictions and caused a transient venular dilatation that was followed a sustained constriction (E). In an LNA-treated preparation, CPA (10 μM) prevented spontaneous constrictions with a sustained constriction (F). The dotted lines indicate the resting diameter of the venule. Scale bars in (B) also applies to (E) and (F).

irrespective of the presence (n = 3) or absence (n = 4) of pretreatment with U-73343 (1 μM).

In the present study, wortmannin, an inhibitor of myosin light chain kinase, was used to prevent tissue distortion (see above). As wortmannin is known to be a potent PI3 kinase inhibitor and may affect Ca^{2+} cycling processes in pericytes, its effects on spontaneous Ca^{2+} transients were examined.

Wortmannin did not change either the frequency (3.3 ± 0.81 min^{-1} in control, 3.5 ± 0.97 min^{-1} in wortmannin, P > 0.05, n = 5) or amplitude (0.91 ± 0.14$\Delta F_t/F_0$ in control, 0.88 ± 0.17$\Delta F_t/F_0$ in wortmannin, P > 0.05) of spontaneous Ca^{2+} transients.

Role of extracellular Ca^{2+} influx in generating spontaneous Ca^{2+} transients of pericytes

Nominally Ca^{2+}-free solution prevented the generation of spontaneous Ca^{2+} transients and reduced basal Ca^{2+} level (0.2 ± 0.035$\Delta F_t/F_0$, n = 5, Figure 9A). Switching from nominally Ca^{2+}-free solution to normal PSS restored spontaneous Ca^{2+} transients and returned the basal Ca^{2+} level to the original level.

SKF96365 (10 μM), a blocker of Ca^{2+} store-operated entry as well as various transient receptor potential channels, gradually suppressed spontaneous Ca^{2+} transients in venular pericytes, and eventually abolished their generation and this was accompanied by a reduction in the basal Ca^{2+} level (.15 ± 0.049$\Delta F_t/F_0$, n = 7, Figure 9B).

YM244769 (1 μM), a blocker for NCX3, did not affect either the frequency (3.7 ± 0.99 min^{-1} in control, 3.6 ± 0.87 min^{-1} in YM244769, P > 0.05, n = 5) or amplitude (0.87 ± 0.28$\Delta F_t/F_0$ in control, 0.84 ± 0.28$\Delta F_t/F_0$ in YM244769, P > 0.05) of spontaneous Ca^{2+} transients in venular pericyte (Figure 9C).

The effect of YM244769 was verified using freshly isolated interstitial cells of the rabbit urethra in which the functional expression of NCX3 has been previously demonstrated (Bradley *et al.*, 2006). YM244769 (0.1 μM, n = 4 or 1 μM, n = 4) abolished Ca^{2+} spontaneous transients of the interstitial cells (Figure 9D).

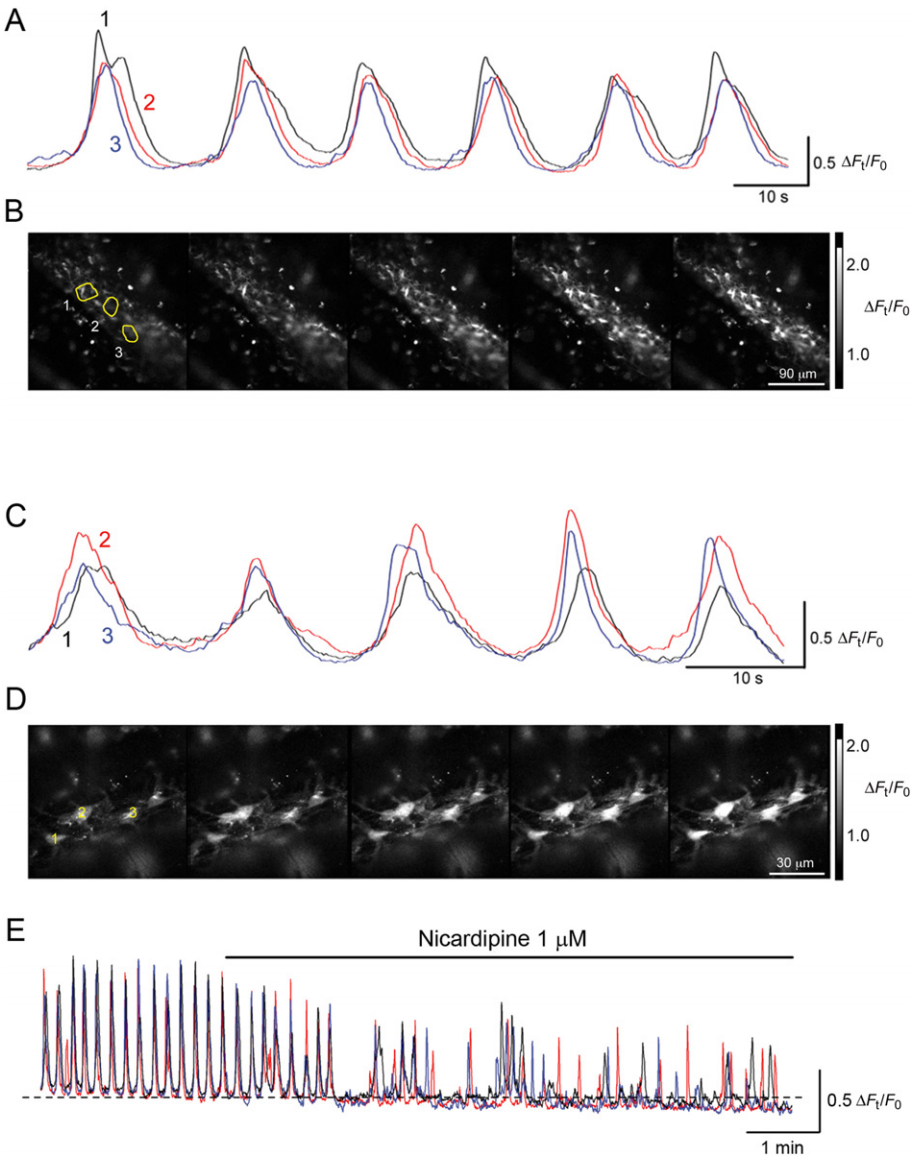

Figure 5

Spontaneous Ca^{2+} transients in the suburothelial venules. Spontaneous Ca^{2+} transients were generated synchronously in three regions of interest (ROIs) in the pericyte network of a suburothelial venule (A). Sequential fluo-4 fluorescent image of spontaneous Ca^{2+} transients demonstrated that synchronous Ca^{2+} transients were generated in three ROIs in the same venule (B). Three pericytes in another venule generated synchronous spontaneous Ca^{2+} transients (C). Sequential fluo-4 fluorescent image of spontaneous Ca^{2+} transients demonstrated that synchronous Ca^{2+} transients were generated in three pericytes in the same venule (D). Frame interval is 1 s in (B) and (C). Number of ROI (B) or cells (D) corresponds to the traces in (A) or (C). In a different venule, nicardipine (1 μM) suppressed spontaneous Ca^{2+} transients and disrupted their synchrony (E).

Discussion and conclusion

In the present study, suburothelial venules displayed spontaneous phasic constrictions. The dominant cell type exhibiting spontaneous Ca^{2+} transients was stellate-shaped pericytes (perivascular cells) which formed an extensive network along the length of venules. Synchronous spontaneous Ca^{2+} transients were developed across this pericyte network, resulting in venular constrictions. Thus, pericytes in the suburothelial venules of bladder appear to be essential machinery driving venular constrictions.

In spontaneously contracting suburothelial venules of the rat bladder, circularly and longitudinally arranged smooth muscle cells were the dominant cells generating spontaneous Ca^{2+} transients, although stellate-shaped pericytes also exhibited spontaneous Ca^{2+} activity (Hashitani *et al.*, 2011). In contrast, both Ca^{2+} imaging and electron microscopy demonstrated that the venular wall of the mouse bladder consists of the pericyte network and mostly lacks smooth muscle cells with the exception of the most proximal portions where circularly arranged spindle-shaped smooth muscle cells were evident in venules >100 μm. Pericytes surrounding capillary

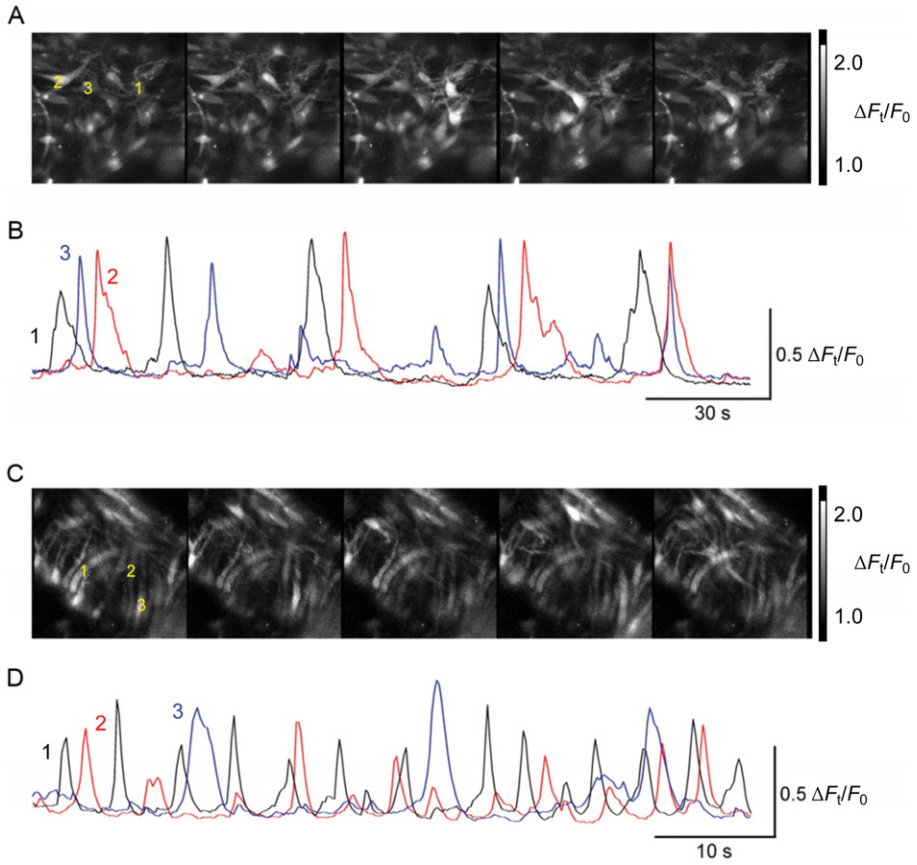

Figure 6

Morphological variation of venular cells generating spontaneous Ca^{2+} transients. Sequential Fluo-4 fluorescent images of spontaneous Ca^{2+} transients in a smaller diameter venule (A). Note that dominant cells exhibiting spontaneous Ca^{2+} transients are stellate-shaped pericytes. Asynchronous Ca^{2+} transients were generated in three pericytes (B). Sequential Fluo-4 fluorescent images of spontaneous Ca^{2+} transients in a large diameter venule (C). Note that dominant cells exhibiting spontaneous Ca^{2+} transients are circularly arranged, spindle-shaped cells. Asynchronous Ca^{2+} transients were generated in three smooth muscle cells (D). Frame interval is 200 ms in (A) and (C). Number of cells (A and C) corresponds to the traces in (B) and (D). Experiments were carried out in the presence of nicardipine (1 μM).

are thought to be contractile and regulate capillary blood flow, and they indeed contract upon the stimulation with several bioactive substances (Hirschi & D'Amore, 1996; Schönfelder *et al.*, 1998; Hamilton *et al.*, 2010). In suburothelial venules of the mouse bladder, it is likely that spontaneous venular constrictions arise from the vigorous contractile properties of pericytes.

Nicardipine reduced the amplitude of spontaneous Ca^{2+} transients in pericytes, and largely suppressed venular constrictions, suggesting that the openings of L-type Ca^{2+} channels cause Ca^{2+} influx to trigger the constrictions. This is an agreement with the finding that freshly isolated retinal pericytes of the rat display inward currents arising from the opening of L-type Ca^{2+} channels (Sakagami *et al.*, 1999). Nicardipine also disrupted synchrony of spontaneous Ca^{2+} transients across the pericyte network as in the rat bladder (Hashitani *et al.*, 2011). Localized, small constrictions spontaneously generated in nicardipine-treated venules may result from asynchronous Ca^{2+} transients in individual pericytes. Thus, activation of L-type Ca^{2+} channels appears to be critical in maintaining functional coupling between pericytes. A reciprocal interaction between cytosolic Ca^{2+} oscillators relying on sarcoplasmic reticulum Ca^{2+} release and membrane conductance carrying inward Ca^{2+} current has been proposed as the mechanism underlying synchronized Ca^{2+} oscillation to initiate vasomotion (Peng *et al.*, 2001). Similar coupled oscillator mechanisms may also underlie long-range synchrony of slow waves in the gastrointestinal tract (Van Helden and Imtiaz, 2003).

As stated previously, pericytes were capable of generating asynchronous spontaneous Ca^{2+} transients in the presence of nicardipine. The residual Ca^{2+} transients were abolished by CPA, 2-APB and U73122, but not ryanodine, suggesting a primary role of $InsP_3$-induced Ca^{2+} release from intracellular Ca^{2+} stores in their generation. Consistently, CPA abolished spontaneous venular constrictions with a dilatation or constriction depending on the availability of background NO, presumably released from endothelium. Thus, the cytosolic Ca^{2+} oscillator in pericytes appears to be very similar to that of ICC (Suzuki *et al.*, 2000; Ward *et al.*, 2000), but different from that of interstitial cells in the urethra, in terms of its sensitivity to ryanodine (Hashitani and Suzuki, 2007). In addition,

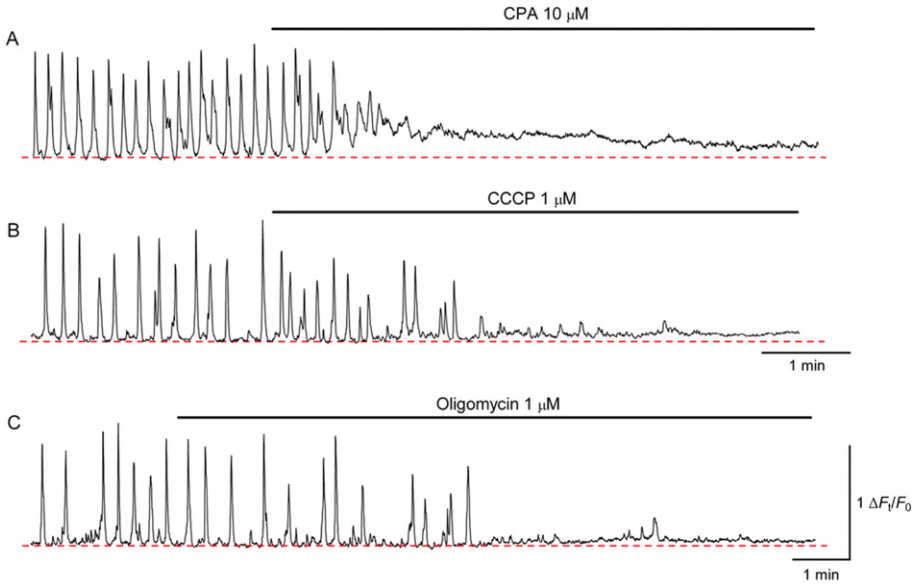

Figure 7

Role of SERCA in generating spontaneous Ca^{2+} transient of pericytes. CPA increased basal Ca^{2+} levels and prevented the generation of spontaneous Ca^{2+} transients (A). In another preparation, CCCP (1 μM) suppressed spontaneous Ca^{2+} transients, and eventually abolished their generation (B). In a different preparation, oligomycin (1 μM) abolished spontaneous Ca^{2+} transients (C). All experiments were carried out in the presence of nicardipine (1 μM). The time scale in (B) also applies to (A). The scale bar to Ca^{2+} fluorescence in (C) applies to all traces.

mitochondrial ATP production, which does not play a critical role in maintaining SERCA activity of ICC (Ward *et al.*, 2000) or interstitial cells of the rabbit urethra (Sergeant *et al.*, 2008), appears to be a major energy source for the operation of SERCA in venular pericytes.

Several studies have indicated that pericytes in the descending vasa recta and retina generate oscillations in cytosolic Ca^{2+} concentrations and Ca^{2+}-activated Cl^- currents (Sakagami *et al.*, 1999; Zhang *et al.*, 2008). In pericytes of suburothelial venules, the $InsP_3$-dependent cytosolic Ca^{2+} oscillator may also interact with Ca^{2+}-activated chloride channels to generate spontaneous transient depolarizations (STDs). STDs may stimulate voltage-dependent $InsP_3$ production (Itoh *et al.*, 1992; Ganitkevich and Isenberg, 1996) resulting in further Ca^{2+} release. However, the reciprocal interaction between the $InsP_3$-dpendent cytosolic Ca^{2+} oscillator and STDs appears to be insufficient to coordinate the diffuse array of cytosolic Ca^{2+} oscillators across the pericyte network, which need to be triggered by Ca^{2+} entry upon the opening of L-type Ca^{2+} channels.

Extracellular Ca^{2+} influx is also required to maintain the cytosolic Ca^{2+} oscillator in pericytes. Spontaneous Ca^{2+} transients and corresponding STICs in interstitial cells of the rabbit urethra are known to rely on Ca^{2+} entry through NCX but not capacitative Ca^{2+} entry (Bradley *et al.*, 2005; 2006). YM-24769, a selective blocker for NCX3 (0.1 or 1 μM; Iwamoto and Kita, 2006), effectively abolished spontaneous Ca^{2+} transients in freshly isolated interstitial cells of the rabbit urethra. Spontaneous Ca^{2+} transients of pericytes were unaffected by YM-24769 (up to 1 μM), but abolished by SKF96365, suggesting that capacitative Ca^{2+} entry channels (CRAC) rather than NCX3 play a fundamental role as a pathway of the Ca^{2+} influx. Consistently, Ca^{2+}-free solution may result in passive Ca^{2+} store depletion preventing the generation of spontaneous Ca^{2+} transients. Nevertheless, the inhibitory action of SKF96365 should be interpreted with caution as this compound is also known to block various transient receptor potential channels. In retinal pericytes, SKF96365 effectively blocked Ca^{2+} permeable non-selective cation channels (Sakagami *et al.*, 1999).

Spontaneous phasic constrictions and associated electrical and calcium activity have been reported in several vascular beds, although whether this activity arises from the intrinsic property of vascular smooth muscle cells themselves or is driven by distinct pacemaker cells remains to be elucidated (Van Helden, 1993; Hill *et al.*, 1999; Haddock *et al.*, 2002). One might expect Kit-positive interstitial cells similar to ICC to be involved in such activity. In rabbit portal vein where two layers of Kit-positive interstitial cells are evident, freshly dispersed single interstitial cells are capable of generating spontaneous Ca^{2+} transients that appear to result from endoplasmic reticulum Ca^{2+} release via ryanodine and $InsP_3$ receptors (Povstyan *et al.*, 2003; Harhun *et al.*, 2006). In the guinea-pig mesenteric artery, spontaneously-active interstitial cells possessing voltage-dependent L-type Ca^{2+} channels are stained by antibodies raised against α-SMA but not Kit receptors, although these cells are non-contractile (Pucovský *et al.*, 2003; 2007). A comparison of the cytoarchitecture of suburothelial venules of the rat and mouse bladders suggests that 'spontaneously active' venular smooth muscle cells may be differentiated from 'pluripotent' pericytes (Hirschi & D'Amore, 1996). When taken together these observations indicate a heterogeneity in the origin of spontaneous activity in various vasculature beds, and the role of pericytes in the contractility of microvasculature may have been underappreciated.

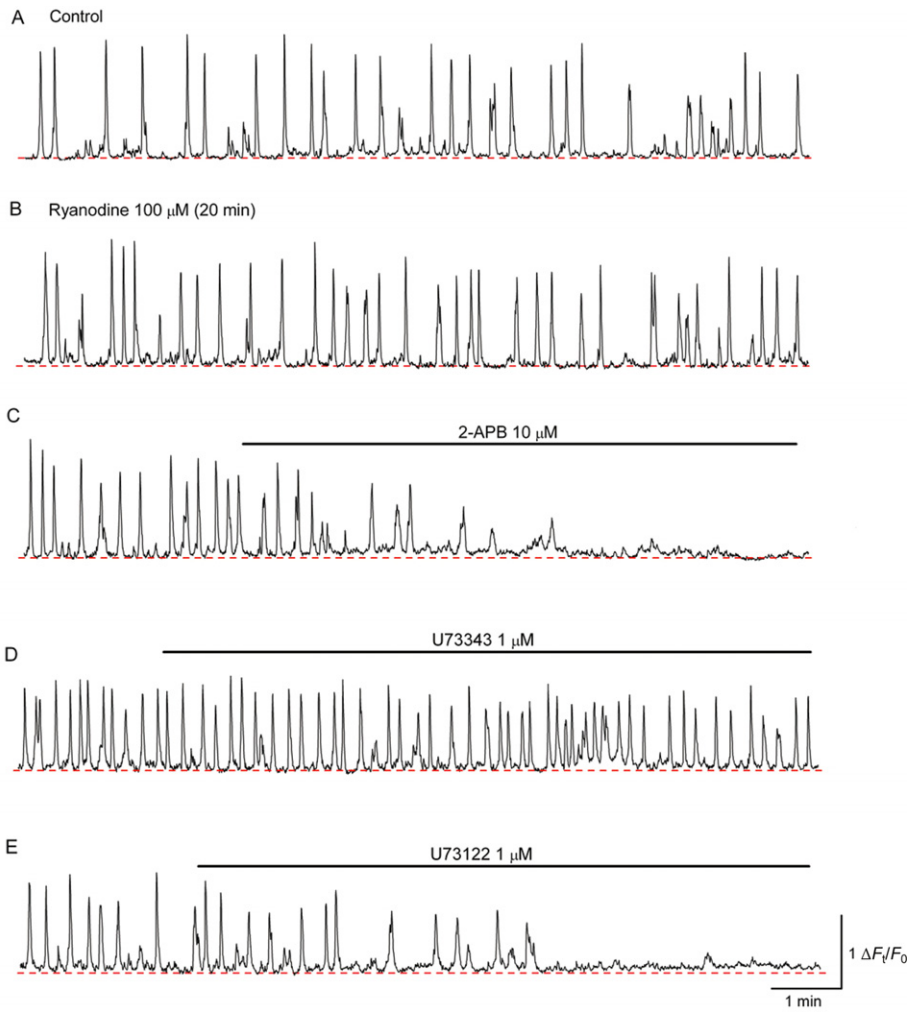

Figure 8

Role of intracellular Ca^{2+} release in generating spontaneous Ca^{2+} transient of pericytes. Spontaneous Ca^{2+} transients were generated in a venular pericyte (A). Pretreatment with ryanodine (100 μM for 20 min) did not affect spontaneous Ca^{2+} transients recorded over the next 10 min in the continued presence of ryanodine (B). Subsequent addition of 2-APB (10 μM) to the same cell as (B) prevented the generation of spontaneous Ca^{2+} transients (C). In another preparation, U73343 (1 μM) failed to inhibit spontaneous Ca^{2+} transients in a venular pericyte (D). In the same cell, subsequent addition of U73122 (1 μM) prevented the generation of spontaneous Ca^{2+} transients (E). All experiments were carried out in the presence of nicardipine (1 μM). The scale bar in (E) applies to all traces.

Pericytes in the suburothelial venules are immunoreactive for α-SMA (Shepro and Morel, 1993) but not Kit (Komuro *et al.*, 1996) or Ano-1/ TMEM16A (Hwang *et al.*, 2009), suggesting that they are distinct from intestinal ICC or Kit-positive interstitial cells in the urinary tract. More recently, another population of cells expressing PDGFRα has been identified in the gastrointestinal tract as well as guinea pig bladder (Iino *et al.*, 2009; Koh *et al.*, 2011). However, the pericytes were not stained by an antibody raised against PDGFRα. In capillaries of several vascular beds, PDGFRβ, which is activated by PDGFB released from endothelium, and NG2, are commonly used as makers for pericytes (Lindahl *et al.*, 1997; Hellström *et al.*, 1999; Ozerdem *et al.*, 2002). The electron microscopy demonstrated frequent close proximity between the pericyte process and endothelial cells, suggesting the likelihood of humoral, even electrical, signal transmission between both cell populations. However, in suburothelial venules of the mouse bladder, the NG2 antibody failed to stain pericytes, while unconvincing PDGFRβ immunoreactivity was detected. Whether PDGFRβ-positive cells in the venule are endothelial cells and/or pericytes is currently uncertain. Presumably, expression of PDGFRβ may be critical for the recruitment or differentiation of pericytes, while the PDGFB/PDGFRβ pathway is non-functional in differentiated 'smooth muscle' phenotype pericytes. Interestingly, both PDGFRβ and NG2 antibodies stained pericytes in capillaries as well as smooth muscle cells in suburothelial arterioles.

Vasomotion in arteries or arterioles has been considered to reduce vascular resistance, and enhance blood flow to facilitate tissue oxygenation (Nilsson and Aalkjaer, 2003). Because in the normal bladder intravesical pressure rises are minimal, it is likely that blood flow of arteries or arterioles is

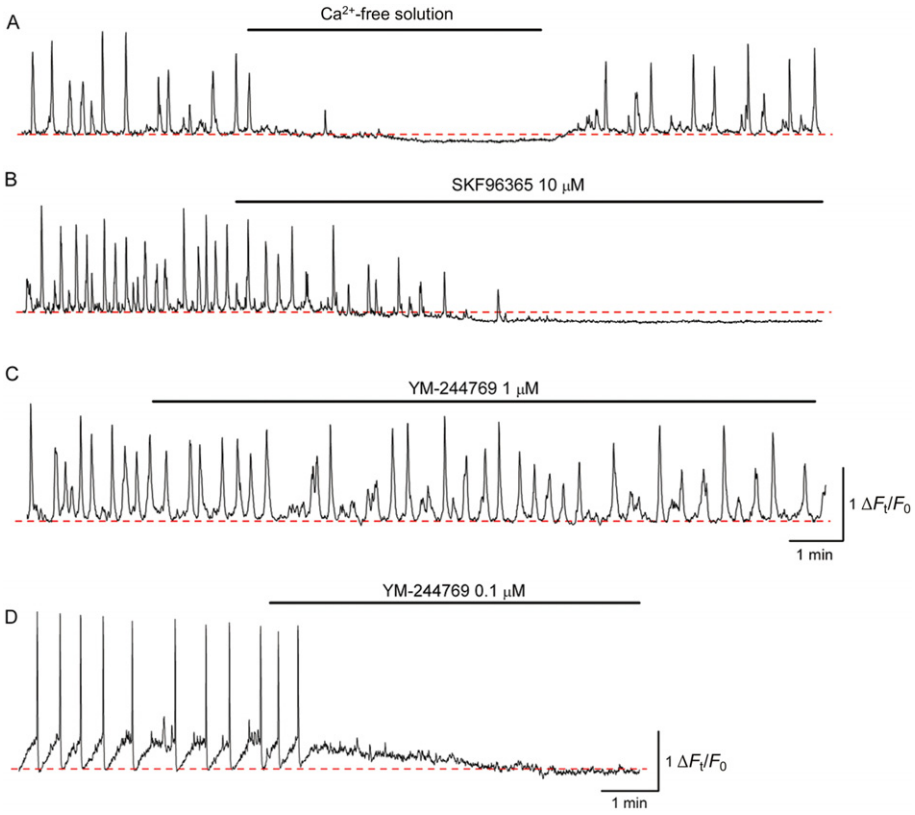

Figure 9

Role of extracellular Ca^{2+} influx in generating spontaneous Ca^{2+} transient of pericytes. Switching from normal PSS to nominally Ca^{2+}-free solution prevented the generation of spontaneous Ca^{2+} transients and reduced the basal Ca^{2+} level (A). Readmission of Ca^{2+} restored spontaneous Ca^{2+} transients and returned the basal Ca^{2+} level to the original level. In another preparation, SKF96365 (10 μM) suppressed spontaneous Ca^{2+} transients, and eventually abolished their generation with a reduction of the basal Ca^{2+} level (B). In a different preparation, YM244769 (1 μM) failed to inhibit spontaneous Ca^{2+} transients in the venular pericyte (C). In contrast, spontaneous Ca^{2+} transients in freshly isolated interstitial cells of the rabbit urethra were abolished in YM244769 (0.1 μM)(D). All experiments were carried out in the presence of nicardipine (1 μM). The scale bars in (C) also apply to (A) and (B).

well maintained. However, even small rises in the intravesical pressure may more readily affect the venular circulation. In addition, suburothelial microvessels undergo considerable rearrangement due to stretch during the bladder filling. Thus, the intrinsic spontaneous constrictions may be beneficial for venular drainage to maintain the suburothelial microcirculation. However, it may be that persistent bladder outlet obstruction or progressive atherosclerosis results in a decrease in spontaneous venular constrictions and consequently an overactive bladder. In addition, the pluripotency of pericytes may contribute to the remodelling of the bladder suburothelium that is commonly seen in an overactive bladder.

Acknowledgements

The authors wish to thank Dr R. J. Lang for his critical reading of the manuscript. This project was supported by Grant-in-Aid for challenging Exploratory Research from JSPS to H. H. (No. 21659377).

Conflict of interest

The authors state no conflict of interest.

References

Alexander SP, Mathie A, Peters JA (2011). Guide to Receptors and Channels (GRAC), 5th edition. Br J Pharmacol 164 (Suppl. 1): S1–S324.

Azadzoi KM, Tarcan T, Siroky MB, Krane RJ (1999). Atherosclerosis-induced chronic ischemia causes bladder fibrosis and non-compliance in the rabbit. J Urol 161: 1626–1635.

Brading AF (1987). Physiology of bladder smooth muscle. In: Torrens M, Morrison JFB (eds). *The Physiology of the Lower Urinary Tract*. Springer-Verlag: London, pp. 161–191.

Bradley E, Hollywood MA, McHale NG, Thornbury KD, Sergeant GP (2005). Pacemaker activity in urethral interstitial cells is not dependent on capacitative calcium entry. Am J Physiol Cell Physiol 289: C625–C632.

Bradley E, Hollywood MA, Johnston L, Large RJ, Matsuda T, Baba A *et al.* (2006). Contribution of reverse Na^+-Ca^{2+} exchange to spontaneous activity in interstitial cells of Cajal in the rabbit urethra. J Physiol 574: 651–661.

Burke EP, Gerthoffer WT, Sanders KM, Publicover NG (1996). Wortmannin inhibits contraction without altering electrical activity in canine gastric smooth muscle. Am J Physiol Cell Physiol 270: C1405–C1412.

Ganitkevich VY, Isenberg G (1996). Effect of membrane potential on the initiation of acetylcholine-induced Ca^{2+} transients in isolated guinea pig coronary myocytes. Circ Res 78: 717–723.

Gosling JA, Kung LS, Dixon JS, Horan P, Whitbeck C, Levim RM (2000). Correlation between the structure and function of the rabbit urinary bladder following partial outlet obstruction. J Urol 163: 1349–1356.

Greenland JE, Brading AF (1996). Urinary bladder blood flow changes during the micturition cycle in a conscious pig. J Urol 156: 1858–1861.

Greenland JE, Brading AF (2001). The effect of bladder outflow obstruction on detrusor blood flow changes during the voiding cycle in conscious pigs. J Urol 165: 245–248.

Haddock RE, Hirst GDS, Hill CE (2002). Voltage independence of vasomotion in isolated irideal arterioles of the rat. J Physiol 540: 219–229.

Hamilton NB, Attwell D, Hall CN (2010). Pericyte-mediated regulation of capillary diameter: a component of neurovascular coupling in health and disease. Front Neuroenergetics 2: 1–14.

Harhun M, Gordienko D, Kryshtal D, Pucovský V, Bolton T (2006). Role of intracellular stores in the regulation of rhythmical $[Ca^{2+}]_i$ changes in interstitial cells of Cajal from rabbit portal vein. Cell Calcium 40: 287–298.

Hashitani H, Suzuki H (2007). Properties of spontaneous Ca^{2+} transients recorded from interstitial cells of Cajal-like cells of the rabbit urethra in situ. J Physiol 583: 505–519.

Hashitani H, Lang RJ, Suzuki H (2010). Role of perinuclear mitochondria in the spatiotemporal dynamics of spontaneous Ca^{2+} waves in interstitial cells of Cajal-like cells of the rabbit urethra. Br J Pharmacol 161: 680–694.

Hashitani H, Takano H, Fujita K, Mitsui R, Suzuki H (2011). Functional properties of suburothelial microvessels in the rat bladder. J Urol 185: 2382–2391.

Hellström M, Kalén M, Lindahl P, Abramsson A, Betsholtz C (1999). Role of PDGF-B and PDGFR-beta in recruitment of vascular smooth muscle cells and pericytes during embryonic blood vessel formation in the mouse. Development 126: 3047–3055.

Hill CE, Eade J, Sandow SL (1999). Mechanisms underlying spontaneous rhythmical contractions in irideal arterioles of the rat. J Physiol 521: 507–516.

Hirschi KK, D'Amore PA (1996). Pericytes in the microvasculature. Cardiovasc Res 32: 687–698.

Hwang SJ, Blair PJ, Britton FC, O'Driscoll KE, Hennig G, Bayguinov YR *et al.* (2009). Expression of anoctamin 1/TMEM16A by interstitial cells of Cajal is fundamental for slow wave activity in gastrointestinal muscles. J Physiol 587: 4887–4904.

Iino S, Horiguchi K, Horiguchi S, Nojyo Y (2009). c-Kit-negative fibroblast-like cells express platelet-derived growth factor receptor alpha in the murine gastrointestinal musculature. Histochem Cell Biol 131: 691–702.

Itoh T, Seki N, Suzuki S, Ito S, Kajikuri J, Kuriyama H (1992). Membrane hyperpolarization inhibits agonist-induced synthesis of inositol 1,4,5-trisphosphate in rabbit mesenteric artery. J Physiol 451: 307–328.

Iwamoto T, Kita S (2006). YM-244769, a novel Na^+/Ca^{2+} exchange inhibitor that preferentially inhibits NCX3, efficiently protects against hypoxia/reoxygenation-induced SH-SY5Y neuronal cell damage. Mol Pharmacol 70: 2075–2083.

Kilkenny C, Browne W, Cuthill IC, Emerson M, Altman DG (2010). NC3Rs Reporting Guidelines Working Group. Br J Pharmacol 160: 1577–1579.

Koh BH, Roy R, Hollywood MA, Thornbury KD, McHale NG, Sergeant GP *et al.* (2011). PDGFRα cells in mouse urinary bladder: a new class of interstitial cells. J Cell Mol Med 16: 691–700.

Komuro T, Tokui K, Zhou DS (1996). Identification of the interstitial cells of Cajal. Histol Histopathol 11: 769–786.

Lang RJ, Hashitani H, Tonta MA, Parkington HC, Suzuki H (2007). Spontaneous electrical and Ca^{2+} signals in typical and atypical smooth muscle cells and interstitial cell of Cajal-like cells of mouse renal pelvis. J Physiol 583: 1049–1068.

Lindahl P, Johansson BR, Levéen P, Betsholtz C (1997). Pericyte loss and microaneurysm formation in PDGF-B-deficient mice. Science 277: 242–245.

McGrath J, Drummond G, McLachlan E, Kilkenny C, Wainwright C (2010). Guidelines for reporting experiments involving animals: the ARRIVE guidelines. Br J Pharmacol 160: 1573–1576.

Neild TO (1989). Measurement of arteriole diameter changes by analysis of television images. Blood Vessels 26: 48–52.

Nilsson H, Aalkjaer C (2003). Vasomotion: mechanisms and physiological importance. Mol Interv 3: 79–89.

Ozerdem U, Monosov E, Stallcup WB (2002). NG2 proteoglycan expression by pericytes in pathological microvasculature. Microvasc Res 63: 129–134.

Peng H, Matchkov V, Ivarsen A, Aalkjaer C, Nilsson H (2001). Hypothesis for the initiation of vasomotion. Circ Res 88: 810–815.

Povstyan OV, Gordienko DV, Harhun MI, Bolton TB (2003). Identification of interstitial cells of Cajal in the rabbit portal vein. Cell Calcium 33: 223–239.

Pucovský V, Moss RF, Bolton TB (2003). Non-contractile cells with thin processes resembling interstitial cells of Cajal found in the wall of guinea-pig mesenteric arteries. J Physiol 552: 119–133.

Pucovský V, Harhun MI, Povstyan OV, Gordienko DV, Moss RF, Bolton TB (2007). Close relation of arterial ICC-like cells to the contractile phenotype of vascular smooth muscle cell. J Cell Mol Med 11: 764–775.

Sakagami K, Wu DM, Puro DG (1999). Physiology of rat retinal pericytes: modulation of ion channel activity by serum-derived molecules. J Physiol 521: 637–650.

Sarma KP (1981). Microangiography of the bladder in health. Br J Urol 53: 237–240.

Schönfelder U, Hofer A, Paul M, Funk RH (1998). In situ observation of living pericytes in rat retinal capillaries. Microvasc Res 56: 22–29.

Sergeant GP, Bradley E, Thornbury KD, McHale NG, Hollywood MA (2008). Role of mitochondria in modulation of spontaneous Ca^{2+} waves in freshly dispersed interstitial cells of Cajal from the rabbit urethra. J Physiol 586: 4631–4642.

Shepro D, Morel NM (1993). Pericyte physiology. FASEB J 7: 1031–1038.

Sun Y, MaLossi J, Jacobs SC, Chai TC (2002). Effect of doxazosin on stretch-activated adenosine triphosphate release in bladder urothelial cells from patients with benign prostatic hyperplasia. Urology 60: 351–356.

Suzuki H, Takano H, Yamamoto Y, Komuro T, Saito M, Kato K *et al.* (2000). Properties of gastric smooth muscles obtained from mice which lack inositol trisphosphate receptor. J Physiol 525: 105–111.

Takasu T, Ukai M, Sato S, Matsui T, Nagase I, Maruyama T *et al.* (2007). Effect of (R)-2-(2-aminothiazol-4-yl)-4′-{2-[(2-hydroxy-2-phenylethyl)amino] ethyl} acetanilide (YM178), a novel selective beta3-adrenoceptor agonist, on bladder function. J Pharmacol Exp Ther 321: 642–647.

Van Helden DF (1993). Pacemaker potentials in lymphatic smooth muscle of the guinea-pig mesentery. J Physiol 471: 465–479.

Van Helden DF, Imtiaz MS (2003). Ca^{2+} phase waves: a basis for cellular pacemaking and long-range synchronicity in the guinea-pig gastric pylorus. J Physiol 548: 271–296.

Ward SM, Ordog T, Koh SD, Baker SA, Jun JY, Amberg G *et al.* (2000). Pacemaking in interstitial cells of Cajal depends upon calcium handling by endoplasmic reticulum and mitochondria. J Physiol 525: 355–261.

Yokoyama O, Yusup A, Oyama N, Aoki Y, Tanase K, Matsuta Y *et al.* (2006). Improvement of bladder storage function by α1-blocker depends on the suppression of C-fiber afferent activity in rats. Neurourol Urodynam 25: 461–467.

Yoshida M, Masunaga K, Nagata T, Satoji Y, Shiomi M (2010). The effects of chronic hyperlipidemia on bladder function in myocardial infarction-prone Watanabe heritable hyperlipidemic (WHHLMI) rabbits. Neurourol Urodyn 29: 1350–1354.

Yoshimura N (2007). Lower urinary tract symptoms (LUTS) and bladder afferent activity. Neurourol Urodynam 26: 908–913.

Zhang Q, Cao C, Zhang Z, Wier WG, Edwards A, Pallone TL (2008). Membrane current oscillations in descending vasa recta pericytes. Am J Physiol Renal Physiol 294: F656–F666.

Supporting information

Additional Supporting Information may be found in the online version of this article:

Video S1 Spontaneous Ca^{2+} transients in a network of pericytes and associated venular constrictions. A fluo-4 loaded suburothelial sheet preparation was pinned flat in a recording chamber.
Video S2 Synchronous Ca^{2+} transients in a network of pericytes. Recorded in a wortmannin (1 μM)-treated preparation.
Video S3 Asynchronous Ca^{2+} transients in venular pericytes. Recorded in the presence of nicardipine (1 μM).